



THE UNIVERSITY *of* EDINBURGH
**School of Physics
and Astronomy**

**Senior Honours Project
DUNE Near Detector to Constrain CP
Violation Measurement Uncertainties**

Paolo Minhas
March 2025

Abstract

DUNE (Deep Underground Neutrino Experiment) is a long baseline neutrino oscillation experiment. One of its key goals is to constrain δ_{CP} . Neutrinos are challenging to detect and uncertainties in beam production, interaction and detection are difficult to constrain. In this report, simulations of the near detectors were used to determine how well measurement uncertainties can be constrained prior to comparing data with the far detector. By comparing reconstructed and true beam energies, we can identify interactions and energy regions where uncertainties strongly affect the spectra. Methods to minimise these effects are explored.

Declaration

I declare that this project and report is my own work.

Signature:

Supervisors: Dr. C. Patrick, Dr M. Nebot-Guinot

Date: 24/03/2025

10 Weeks

Contents

1	Introduction	2
2	Background	2
2.1	CP Violation and Neutrino Oscillations	2
2.2	The Beam and Neutrino Production	5
2.3	The Near Detector Complex	6
2.4	Neutrino Interactions in the detector	10
2.4.1	Coherent (COH) Scattering	10
2.4.2	Quasi-Elastic Charged Current (CCQE) Scattering	10
2.4.3	Resonant Pion Production (RES)	11
2.4.4	Deep Inelastic Scattering (DIS)	11
2.4.5	Meson Exchange Current (MEC) Interaction	12
2.4.6	New Cross-Section Measurements	12
2.5	Interaction Uncertainties	13
3	Simulation and Analysis Techniques	14
3.1	Event Selection	14
3.2	Reconstruction	15
3.3	Code	15
4	Analysis and Discussion	16
4.1	Neutrino Energy Spectra	16
4.2	Types of Interaction	18
4.3	Approaches to Reconstruction	20
4.4	Truth versus Reconstructed Energy	22
5	Conclusions	24
A	The PNMS Matrix and Oscillation Probabilities	27

1 Introduction

Charge-conjugation and parity-reversal (CP) violation represents an asymmetry within interactions (in this report the focus is the leptonic sector, meaning the interactions involve leptons). This leads to the observed matter-antimatter asymmetry in the universe, via a hypothetical process called leptogenesis [1], not discussed in this report. CP violation in the leptonic sector can be effectively probed by examining neutrino oscillations – where neutrinos oscillate between flavours, which corresponds to the quantum number three generations of leptons, as they travel.

The DUNE (Deep Underground Neutrino Experiment) detectors – both the near detector (ND) complex at the neutrino beam source and the far detector (FD) complex around 1300km away – are able to measure the proportions of neutrino flavours present in the beam in those respective locations. Therefore by comparing the amounts of a given flavour, such as electron neutrinos, at the near and then far detector, that the amount of neutrinos that have oscillated from another flavour can be calculated as the difference (in reality this is far more complicated). We can compare the oscillation probabilities of an identical process for antielectron neutrinos. Any differences between them suggest CP violation, as under CP symmetry the processes should be identical. The proportions can be used to calculate a value for the CP phase angle (δ_{CP}) which characterises the extent of the CP violation.

This report will analyse simulated ND energy spectra from neutrino and antineutrino interactions, which are important as they determine the initial beam composition, before any statistically significant proportion of the beam can oscillate. This is the purpose of the FD. Ensuring accurate measurements of the beam at the ND greatly reduces uncertainties when obtaining the oscillation data from the far detector. There are however many challenges with this, that will be outlined by this report, ranging from the beam flux to the detectors themselves.

This report examines how the DUNE collaboration will minimise uncertainties at the ND, how the improved data can be used to find a value for δ_{CP} , and how the detectors will be improved in the future to find a value with higher accuracy. Simulations of the ND are run with different beam configurations, to find the most effective beam and detector arrangements for obtaining a value of δ_{CP} , and the interactions with the greatest CP violation are analysed. Before examining the DUNE detector simulations, it is worth exploring the theory of neutrino oscillations and CP violation in the leptonic sector.

2 Background

2.1 CP Violation and Neutrino Oscillations

CP violation is seen through differences between matter and antimatter interactions at DUNE. It was first discovered experimentally by Cronin and Fitch in 1964 [3] in neutral Kaon mixing. Sakharov used this to explain the baryon asymmetry in the universe 3 years later [4], and this lead to the theory of leptogenesis [1] to generate lepton number asymmetry and convert this to baryons [5]. Explaining the extent of the matter-antimatter imbalance in the universe provides a motivation to find CP violation in the leptonic sector.

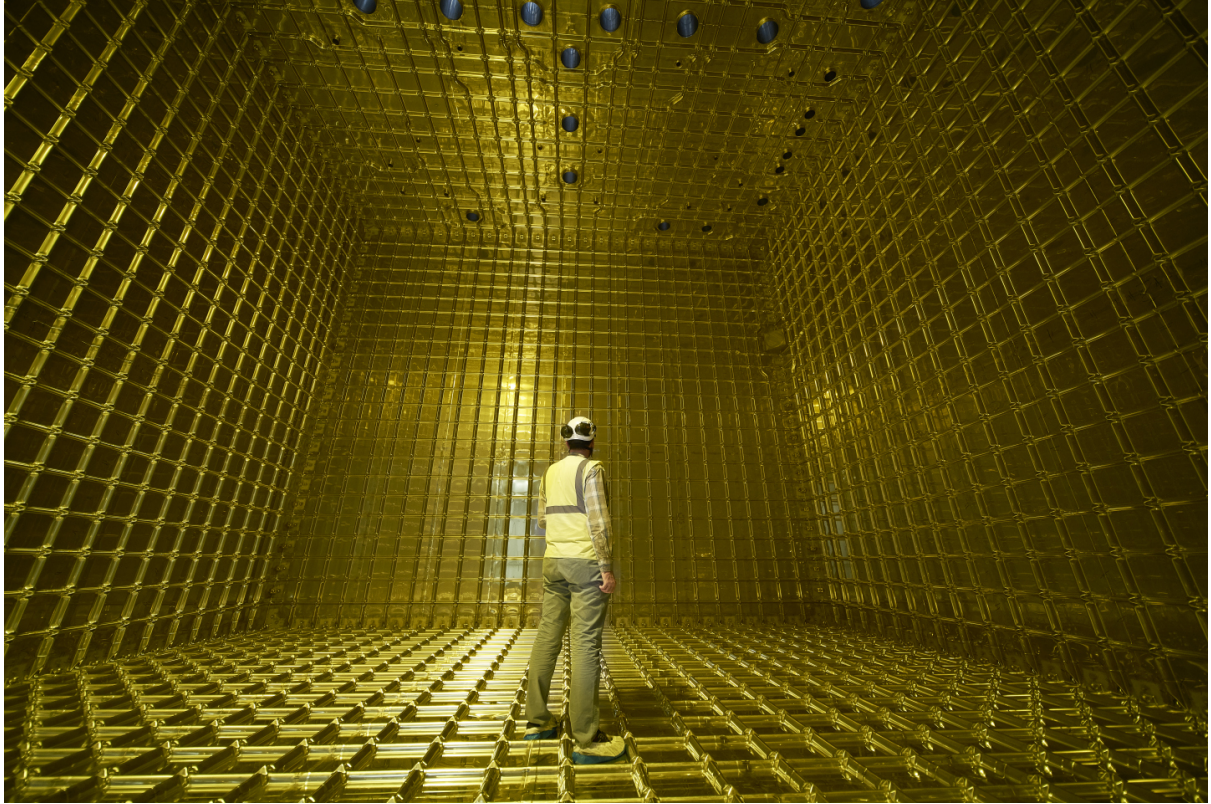


Figure 1: The inside of a Liquid Argon Time Projection Chamber, used to detect neutrinos at ProtoDUNE (a practice for DUNE) in CERN. DUNE will use this type of neutrino detector at the ND and FD, as it can detect many events due to a high density of relatively heavy argon nuclei. Figure retrieved from [2].

A neutrino is a subatomic particle (a left-handed¹ lepton) with a spin of $\frac{1}{2}$. Its existence was first postulated by Pauli in 1930 [6] to conserve momentum and spin in β decays and further elaborated upon by Fermi in 1934 [7]². Neutrinos interact only via the weak force and very weakly via gravity due to their small mass. It is not yet fully understood whether they are Dirac or Majorana particles³. Neutrino oscillations are a quantum mechanical phenomenon that arises due to lepton flavour mixing—neutrinos can change flavour as they travel—as first theorised by Pontecorvo in 1967 [12]. Flavour states correspond to the lepton’s interactions via the weak force—there are three (one for each generation): electron, muon and tau. The quantum number (in this case lepton

¹Handedness refers to the direction of spin relative to the direction of propagation—in this case left handed means the spin is in the opposite direction to the direction of propagation.

²Fermi’s groundbreaking paper on the weak force and the neutrino was written in Italian—an English translation is available at [8].

³Dirac particles mean neutrinos and antineutrinos are distinct and obtain mass via standard model processes (via interaction with the Higgs field), whereas Majorana neutrinos [9] are their own antiparticles [10]. DUNE will in fact search for Majorana neutrinos by searching for neutrino-less beta decay—a process in which the neutrino produced in beta decay is virtual acts as an exchange particle as it is own antiparticle and therefore no neutrinos are produced when two beta decay processes occur simultaneously [11].

number) represents each state and is mostly conserved in weak interactions, being violated by neutrino oscillations.

Neutrinos propagate through space not as flavour eigenstates, but as mass eigenstates (it is worth noting that as a result of this, neutrinos must have mass). The probability of a neutrino being detected in a given flavour state changes over time—the mass eigenstates are superpositions of the flavour eigenstates. Flavour eigenstates $|\nu_\alpha\rangle$ ($\alpha = e, \mu, \tau$) and mass eigenstates $|\nu_i\rangle$ ($i = 1, 2, 3$) are related by:

$$|\nu_\alpha\rangle = \sum_i U_{\alpha i} |\nu_i\rangle, \quad (1)$$

The relationship between the mass eigenstates and flavour eigenstates is given by the 3x3 unitary, complex Pontecorvo-Maka-Nakagawa-Sakata (PMNS) matrix. $U_{\alpha i}$ represents the matrix elements of the PNMS matrix:

$$\begin{bmatrix} \nu_e \\ \nu_\mu \\ \nu_\tau \end{bmatrix} = \begin{bmatrix} U_{e1} & U_{e2} & U_{e3} \\ U_{\mu 1} & U_{\mu 2} & U_{\mu 3} \\ U_{\tau 1} & U_{\tau 2} & U_{\tau 3} \end{bmatrix} \begin{bmatrix} \nu_1 \\ \nu_2 \\ \nu_3 \end{bmatrix} \quad (2)$$

When any off-diagonal matrix elements are non-zero, as well as non-zero differences between ν_1, ν_2, ν_3 mass states—neutrino oscillations can occur. The oscillation frequency is proportional to the neutrino mass-squared differences:

$$\Delta m_{ij}^2 \equiv m_i^2 - m_j^2$$

Assuming the neutrinos are Dirac fermions (see Appendix), the PNMS matrix is able to be parametrised with 3 mixing angles (θ_{12}, θ_{13} and θ_{23}) and a complex phase δ_{CP} :

$$\sin^2 \theta_{12} = \frac{|U_{e2}|^2}{1 - |U_{e3}|^2} = 0.307^{+0.012}_{-0.011} \quad (3)$$

$$\sin^2 \theta_{13} = |U_{e3}|^2 = 0.561^{+0.012}_{-0.015} \quad (4)$$

$$\sin^2 \theta_{23} = \frac{|U_{\mu 3}|^2}{1 - |U_{e3}|^2} = 0.02195^{+0.00054}_{-0.00058} \quad (5)$$

These values are a global fit of experimental data taken from [13] and [14], assuming normal ordering (see Table 1). The CP-violating phase δ_{CP} is defined as:

$$\delta_{CP} = -\arg(U_{e3}) \quad (6)$$

Assuming none of the matrix elements disappear and δ_{CP} is not 0 or π , the oscillation probabilities are not symmetrical in CP transformations:

$$P(\nu_\alpha \rightarrow \nu_\beta) \neq P(\bar{\nu}_\alpha \rightarrow \bar{\nu}_\beta), \quad \alpha, \beta = e, \mu, \tau, \quad \alpha \neq \beta. \quad (7)$$

Determining neutrino mass ordering (whether ν_3 is the heaviest or lightest neutrino, in normal and inverted ordering respectively) is a goal for DUNE.

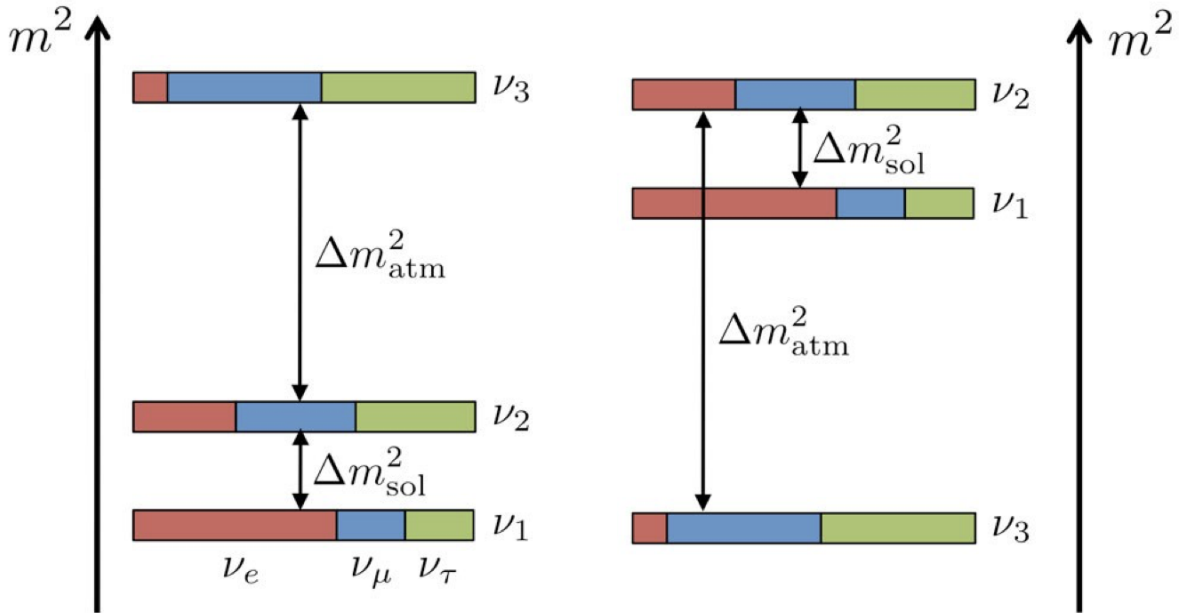


Figure 2: The neutrino mass ordering: normal ordering is shown on the left and inverted on the right. The mass splitting terms are equal in both scenarios, the only difference being whether ν_1 is heaviest or lightest. Mass increases vertically in this diagram. The flavour state superpositions are shown as blocks of colour. Taken from [15].

2.2 The Beam and Neutrino Production

The DUNE detectors use a beam from the Long Baseline Neutrino Facility (LBNF) at Fermilab, Illinois. This extracts a proton beam from the MI-10 section of the Fermilab Main Injector using “single-turn” extraction. This means a fast kicker magnet extracts the whole batch of protons in a short burst, around μs long, instead of over many cycles. Guided by magnets, it produces a neutrino beam angled towards the Sanford Underground Research Facility (SURF) in South Dakota 1300km away. This beam is expected to be the highest power neutrino beam in the world. The primary proton beam is in the 60 – 120 GeV range, and the beam power will be in the range 1.03 – 1.20 MW [16]. In the future, the Proton Improvement Plan, phase II (PIP-II) will double the beam power. The protons hit a graphite target – this interaction produces mesons such as pions and kaons. The charged mesons are focused and sign selected by the magnetic horns (meaning that one charge orientation of meson is funnelled away, and the opposite charge is focused into a beam of mostly coherent charge). The magnetic horns can be put into two different arrangements: forwards and reverse horn current (FHC and RHC respectively) [17]. FHC provides a neutrino rich beam and RHC an antineutrino beam – thus allowing comparison between the two at the ND. The beam will be optimised to maximise sensitivity to CP violation. There are 3 magnetic horns and the graphite target is cooled with water and helium to reduce heating effects. These mesons have short half-lives and quickly decay in the 221m long decay pipe into muons and neutrinos. At the end of this pipe, there

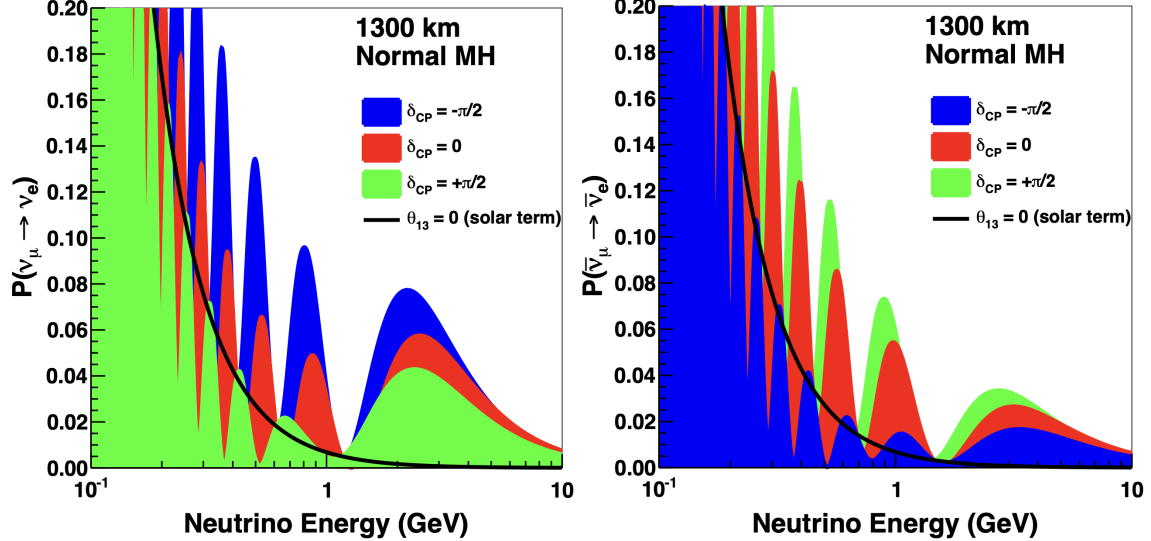


Figure 3: DUNE has a baseline of 1300km—the appearance probability is shown as a function of neutrino energy at DUNE. The figure on the left shows this for neutrinos, whereas the right shows this for anti neutrinos. The black line shows where $\theta_{13} = 0$. At lower energies it becomes easier to determine the value for δ_{CP} , as it more greatly affects amplitude and phase in this region. Both graphs assume normal mass ordering. Figure taken from [15].

is an absorber to remove residual hadrons (therefore all of the mesons), resulting in the final wide band neutrino beam. The beam is required to be wide band (covering a range of energies) to cover the energies of the first and second neutrino oscillation maxima (2.4 and 0.8 GeV) [16].

There are several features to the beam that complicate matters. The proton interaction with graphite results in a range of particles as seen in Table 1. The final beam is therefore not just made up of one flavour of neutrinos, or leptons due to this. The particles can also interact with the materials in the beam production such as the pipes, and as the beam is used for decades, the amount of beam energy deposited in surrounding infrastructure will damage equipment, unless this is accounted for in the building of it. Around 40% of the power of the beam will be deposited into the target (and the shielding around it), 19% into the decay pipe and 33% into the absorber. It is only 8% of the beam power that remains, not all of which is in the neutrino beam [16]. This dumping of high energy radiation is accounted for in the design to minimise its impact on the local area, and on results. There are also facilities for monitoring and altering the beam. There are muon detectors in the muon alcove (just after the hadron absorber) that give details of beam intensity, direction and the muon spectrum. The flux of all muons is measured using ionisation detectors made of diamonds or silicon. The beam orientation can be altered and therefore there are detectors to measure signal intensity.

2.3 The Near Detector Complex

The information in this section was compiled from the DUNE Technical Reports [17][19].

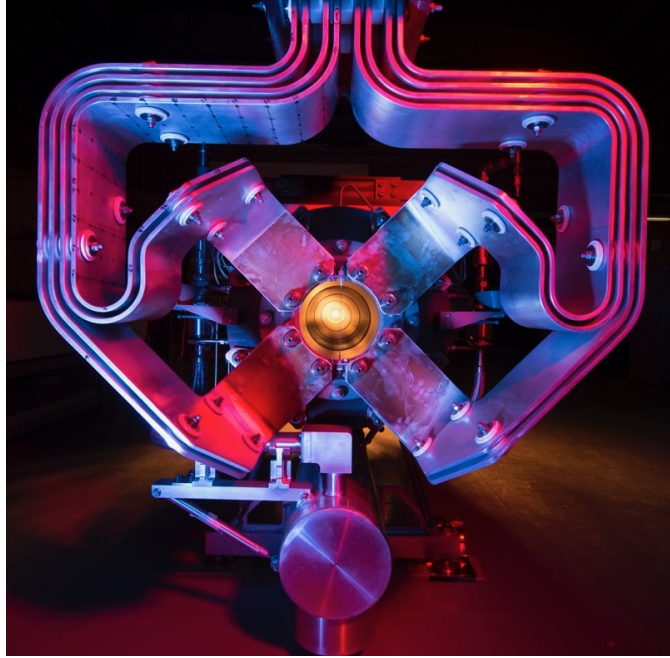


Figure 4: A magnetic horn used at DUNE.

The Near Detector Complex acts as a control for the experiment – providing the initial neutrino energy spectra before the neutrinos have oscillated. It will constrain systematic errors by measuring the initial ν_μ , ν_e , $\bar{\nu}_e$ and $\bar{\nu}_e$ energy spectra. The resulting energy spectra are convolutions of the flux, cross section and the response of the detector (energy dependent), for ν_μ , ν_e , $\bar{\nu}_e$ and $\bar{\nu}_e$ respectively. These three factors will be independently constrained at the ND, and these constraints will be used to improve simulations of the FD energy spectra which are used to calculate oscillation parameter by performing a fit to the obtained FD data. The near detector has programs which do not involve the FD [20]. These experiments will probe quantum chromodynamics and electroweak physics, searching for interactions including sterile neutrinos [21] and dark photons [22]. This paper will however not detail these experiments.

To constrain systematic errors and provide optimal spectra for use at the FD, there are several requirements for the ND the DUNE collaboration has focused on. It must be able to predict the neutrino energy spectrum at the FD with systematic errors that are small enough to still be able to measure the CP violation. The argon interactions must be measured, so uncertainties in nuclear interaction modelling can be reduced, and the flavour of neutrino interacting can be identified. The neutrino energy must be measured from CC events and must be usable with FD data. The neutrino cross section must be measured and constrained to make good predictions for FD data. The neutrino fluxes must be measured to measure the cross sections and constrain the beam model. Taking data from a range of different flux values can prevent systematic uncertainties on the energy reconstructions of the neutrino interactions. Finally, by monitoring the beam in real time, small changes in the beam energy spectrum can be accounted for when taking the oscillation measurements, and the beam can be adjusted.

The ND complex is made up of three sections: The Liquid Argon Time Projection

Particle	Lifetime (s)	Decay Products	Proportion in Beam
π^+	2.60×10^{-8}	$\mu^+ \nu_\mu$	~60% of the beam
π^-	2.60×10^{-8}	$\mu^- \bar{\nu}_\mu$	~30% of the beam
K^+	1.24×10^{-8}	$\mu^+ \nu_\mu$ or $\pi^+ \pi^0$	~5-10% of the beam
K^-	1.24×10^{-8}	$\mu^- \bar{\nu}_\mu$ or $\pi^- \pi^0$	~1-3% of the beam
K_L^0	5.1×10^{-8}	$\pi e \nu_e$	very small proportion
K_S^0	8.95×10^{-11}	$\pi^+ \pi^-$	very small proportion
μ^+	2.20×10^{-6}	$e^+ \nu_e \bar{\nu}_\mu$	secondary
μ^-	2.20×10^{-6}	$e^- \bar{\nu}_e \nu_\mu$	secondary

Table 1: Proportions of common particles formed in the beam. This data is taken from NA61/SHINE in CERN [18], which uses a similar beam for the purpose of modelling beams like DUNE’s.

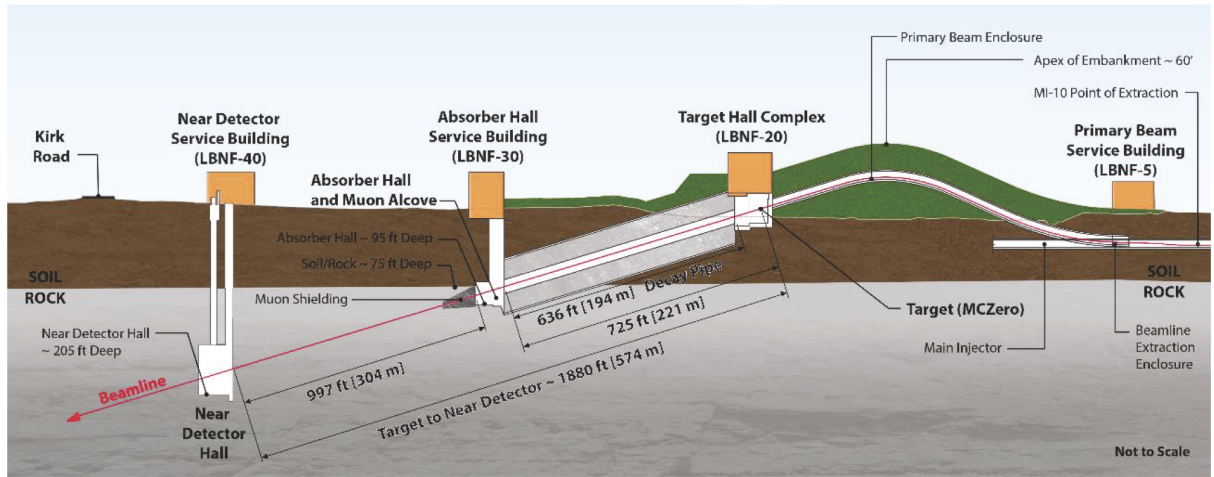


Figure 5: A schematic of the LBNF beam production facilities and DUNE ND complex at Fermilab, Illinois. It can be seen that mesons have 221m to decay into neutrinos before being absorbed. The distance that neutrinos have to travel to the ND is relatively short, to minimise oscillation.

Chamber (LArTPC), the Multipurpose Detector (MPD) and the System for on-Axis Neutrino Detection (SAND – a beam monitor). The first two detectors are able to move off the beam axis, changing the flux spectrum detected (this is referred to as the DUNE-PRISM capability – DUNE Precision Reaction-Independent Spectrum Measurement). This report will focus on simulations of the LArTPC and part of the MPD.

The LArTPC is an arrangement of 35 time projection chambers (TPCs), surrounded by liquid argon, which must be cryogenically cooled due to the relatively low boiling point of argon. The target nucleus in the detector is the same as that of the FD, reducing systematic errors due to the detector and sensitivity to nuclear effects (same nucleus). The detector has many other similarities in construction and use to the FD, however due to the beam intensity being higher at the ND, there are differences. The detector is large: it aims to record $10^8 \nu_\mu$ -CC events per year and this also aids with hadron containment. There are drawbacks to the detector however, such as lack of muon containment for

muons with a momentum greater than $0.7\text{GeV}/c$. Recording muon momentum is crucial for calculating neutrino energy, therefore the MPC, lying downstream from the LArTPC, contains a magnetic spectrometer to measure the momentum and charge sign of the muons.

The MPD contains a high-pressure gaseous argon TPC (HPgTPC) enclosed by an electromagnetic calorimeter (ECAL). The density is lower than in the LArTPC (as it uses Ar gas) allowing detection of lower momentum protons and reductions in secondary interactions (which in turn helps identify primary interactions and model secondary interactions in the LArTPC by comparison). It has different systematic errors to the LArTPC, so by using both detectors overall uncertainties are decreased. The high pressure means many events ($2 \times 10^6 \mu_\nu\text{-CC}$ per year) will be collected.

DUNE-PRISM allows the LArTPC and MPD detectors to move off axis (the axis of the beam). As the angle of incidence of the beam increases as the detectors move further off axis, the beam is more monochromatic and the mean energy decreases. Taking a linear combination of the different beam fluxes produces a neutrino energy spectrum close to that expected at the FD. This reduces systematic uncertainties due to the differences in spectra that would otherwise be seen between the ND and FD.

SAND is primarily made up of a 3D scintillator tracker (1cm³ cubes of plastic which scintillate when neutrinos are detected), which can determine neutrino flux. It is used as a cross-check with the LArTPC.

The LAr and GAr detectors use charged grids of parallel wires arranged in different directions around the detector to measure charged particles like electrons that come from reactions and allow a 3D track of the reaction to be produced. By using machine learning and other more methodical empirical methods, these tracks are analysed to determine what type of interaction has occurred. Overall, all the ND components combine to identify neutrino flavour and energy in CC interactions to create a prediction for the FD, which puts constraints on the oscillation parameters when compared to FD data; thus measuring neutrino oscillation.

By compounding all the possible uncertainties on a given data point it is possible to come to the following equation, when finding the final data for neutrino oscillation:

What we measure	What we want to know
$R_{\mu \rightarrow e}(E_{\text{rec}}) = N \int dE_\nu \Phi_\mu(E_\nu) P_{\nu_\mu \rightarrow \nu_e}(E_\nu) \sigma_e(E_\nu, E_{\text{rec}}) \epsilon_e(E_\nu)$	
Oscillated neutrinos detected, as a function of measured energy	Flux (energy spectrum) of unoscillated neutrinos
	Probability of a neutrino oscillating, as a function of its true energy
	Interaction cross section - the probability a neutrino interacts and the amount of its energy we can detect
	Detector efficiency - the chance of successfully detecting a neutrino if it interacts

Figure 6: The impact of the uncertainties can be seen on the measured neutrino oscillation at the FD. Figure taken from [23].

The detector efficiency of the ND must be found to get data for oscillation, but this

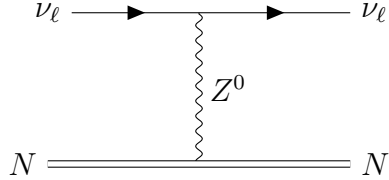


Figure 7: A neutrino of arbitrary flavour interacts with a nucleus via the weak interaction. A neutral Z^0 boson exchanged between the neutrino and nucleus.

can only be known once operational. The uncertainties in detection originate from events escaping the detector, or not being detected at all however they mostly originate from interaction uncertainties.

2.4 Neutrino Interactions in the detector

Neutrinos are difficult to detect as they very rarely interact. They are not directly visible themselves—so must be detected via interactions with other particles, in this case argon nuclei, and then using kinematics detected by finding missing energy or by the interaction products. There are a large range of neutrino energies present in the beam, and this leads to multiple types of neutrino scattering occurring. The majority of the interactions with the nuclei are with neutrons rather than protons. This is due to weak interactions favouring neutrons in CC interactions as protons are not as energetically available to interact with, the neutron ratio in an argon nucleus (22n, 18p) and that neutrinos can interact with protons via NC (neutral current, with a Z^0 boson) interactions, but these are detected less in the detector as they are extremely difficult to measure. The most common forms of neutron-neutrino scattering will be explored in this report. CP symmetry would imply the same processes occur with anti-neutrinos with opposite charge conjugation and parity.

2.4.1 Coherent (COH) Scattering

Coherent scattering is an NC weak interaction. First predicted theoretically in 1974 [24] and proven experimentally 43 years later [25], neutrinos interact with the nucleus as a whole, causing a small amount of recoil on the nucleus [26]. This is the only way to detect the interaction, making it challenging to detect. DUNE has a high energy beam, but at the lower energy end of the spectrum, NC interactions may be visible—however DUNE has no dedicated detector for this currently planned.

2.4.2 Quasi-Elastic Charged Current (CCQE) Scattering

A neutron in a nucleus is bound in a nuclear potential, moving, meaning it is neither at rest nor free. CCQE refers to a charged current (via the weak force, exchanging a W^\pm boson) quasi-elastic (elastic-like so that no additional hadrons are produced and the interaction occurs with a single nucleon) interaction [27]. It occurs at lower energies (1-10GeV at DUNE), and involves the neutrino interacting with a neutron producing a proton and a lepton of the same flavour as the neutrino. Assuming CP-symmetry an antineutrino interacts with a proton producing an anti-lepton and a neutrino. If CP

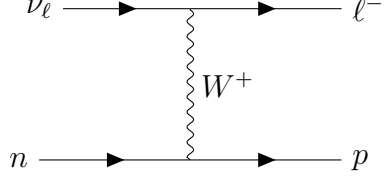


Figure 8: A neutrino becoming a charged lepton in a CCQE weak interaction with a neutron.

violation exists in this interaction, then a different probability would be expected for the equivalent neutrino case.

2.4.3 Resonant Pion Production (RES)

Resonant Pion Production (RES) works in a similar way to CCQE, however it occurs at higher energies where instead of producing a proton and lepton, the proton is replaced by a Δ particle which is a resonance of 3 quarks (combinations of up and down quarks in an excited state) [28]. This can occur with both protons and neutrons:

$$\nu_\mu + p \rightarrow \mu^- + \Delta^{++}, \text{ followed shortly by: } \Delta^{++} \rightarrow p + \pi^+ \quad (8)$$

$$\nu_\mu + n \rightarrow \mu^- + \Delta^+, \text{ followed shortly by: } \Delta^+ \rightarrow n + \pi^+ \quad (9)$$

$$\bar{\nu}_\mu + p \rightarrow \mu^+ + \Delta^0, \text{ followed shortly by: } \Delta^0 \rightarrow p + \pi^- \quad (10)$$

$$\bar{\nu}_\mu + n \rightarrow \mu^+ + \Delta^-, \text{ followed shortly by: } \Delta^- \rightarrow n + \pi^- \quad (11)$$

This interaction produces the same products as CCQE with an additional pion, therefore it has a distinct signature to be detected when analysing tracks.

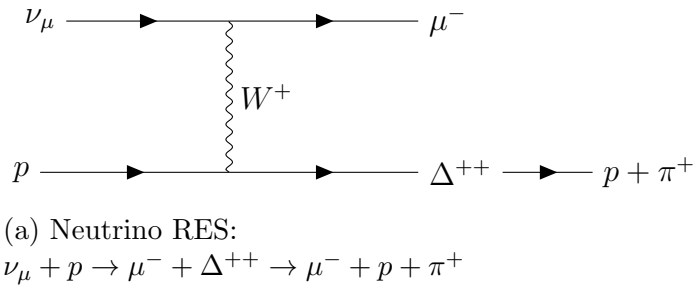


Figure 9: Charged-current resonant scattering for neutrinos.

2.4.4 Deep Inelastic Scattering (DIS)

It is possible to have DIS interactions that are NC or CC. In DIS interactions, high energy neutrinos and antineutrinos interact with a nucleon, causing a hadronic shower (the nucleon breaks up and a shower of hadrons is released). In NC interactions the neutrino remains in the final state, whereas they become leptons in CC interactions. Combined with understanding RES and CCQE interactions, a better picture of the neutrino cross section can be obtained, and at DUNE nuclear effects will be probed by looking at quark-gluon interactions in high energy DIS interactions [29].

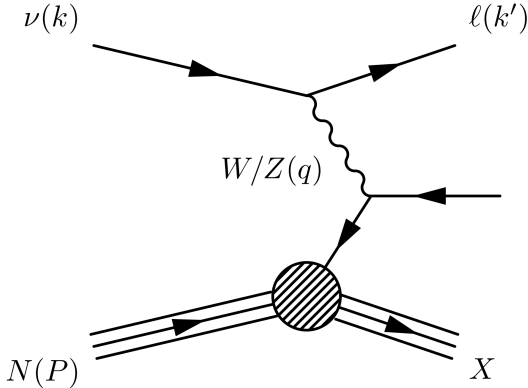


Figure 10: Deep inelastic scattering releasing a hadronic shower. Figure taken from [29].

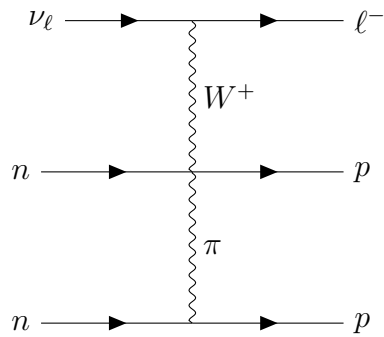


Figure 11: MEC interaction.

2.4.5 Meson Exchange Current (MEC) Interaction

Meson Exchange Current (MEC) interactions involve neutrinos scattering off nucleons that are part of a correlated nucleon pair—a virtual meson such as a pion acts as an exchange particle in this case. These events can appear similar to CCQE, but include additional nucleons and therefore can lead to substantial challenges when performing reconstruction of the neutrino energy.

MEC interactions can lead to 2p2h—a ‘Two-Particle Two-Hole’ state [30]. This is where two nucleons are knocked out of the nucleus by the neutrino simultaneously. Not all 2p2h final states are caused by MEC interactions—however they are a large contribution. These phenomena have been implemented into the Monte Carlo models used to simulate data in this report.

2.4.6 New Cross-Section Measurements

Neutrino cross-section measurements have changed in recent years—recording data for each interaction mode has been replaced by more objective data. This means moving away from previous corrections that were very dependent on each interaction mode, to determine the final states observed by the detectors. The CCQE cross section has mostly been substituted for looking for a final state with one μ and no pions, known as CC0 π (also known as CCQE-like). This state has a mix of contributions, as will be analysed

in this report. There are contributions from CCQE, 2p2h and from π production where π is absorbed so it appears as if there was no π . There are also CC1 π measurements. The dominant interactions vary by energies involved resulting in different CC1 π measurements, for example at high energy DIS and high mass resonances dominate whereas at lower energy the $\Delta(1232)$ resonance (a type of RES) dominates—a resonance with an excited nucleon that becomes a Δ particle, it is the lowest level resonance (in the first excited state). It generally exists at energy levels between QE and DIS scattering, where RES scattering is.

2.5 Interaction Uncertainties

These interactions make up the majority of interactions detected at the ND—as is aimed to be shown by simulation in this report. There are however uncertainties involved with how these interactions are identified, and most crucially differentiated between each other. The most useful data to find δ_{CP} is obtained from CC events as these give the neutrino flavour. The CCQE RES DIS and MEC interactions have similar final states: if pions or hadrons produced in the interactions are absorbed or not detected then large uncertainties in identifying the interaction are introduced. There are many complex interactions involving many particles in the final state, most crucially secondary interactions (especially prevalent in the LArTPC due to the higher density than the GArTPC) can lead to changing the signature and tracks, as well as energy losses. The binding energy of nuclei must be considered, as without this the interaction cross sections will be lower than expected. Nucleons moving can change final state kinematics. 2p2h final states look like CCQE with extra nucleons involved—this can affect energy reconstruction. Short range correlations between nucleons (as in MEC) increase uncertainty in neutrino momentum before the interaction; they distort the energy spectrum making neutrino energy appear lower than reality.

Before describing the experimental procedure, it would prove useful to summarise what has been detailed so far. The neutrino beam is made from protons, that become mesons which decay to neutrinos. These then interact with Ar nuclei in the LArTPC and GArTPC, via a variety of interactions as the beam is wide band. The tracks from these interactions are recorded by the ND and analysed, then sorted into types of interaction. This data will then be compared to the FD to find relevant PNMS matrix elements in order to find δ_{CP} , and other important parameters such as mass splitting terms and the neutrino oscillation parameters. There are uncertainties in the flux of the beam, the beam contents and production, the interactions which occur in the detector and in the ability of the detector to identify and record these accurately. With so many sources of uncertainty, DUNE has been optimised to reduce these and, where possible, uses Monte Carlo simulation to account for these.

3 Simulation and Analysis Techniques

This report will analyse simulations of the NDLaR and the NDGAr (the latter is a part of the MPD). The simulations were made using GENIE—a ROOT⁴ based Monte Carlo Neutrino Generator [32]. GENIE is used globally to model neutrino programs and is used at DUNE as well as other Fermilab detectors to model events.

The simulation is composed of ‘truth’ and ‘reconstructed’ data. Truth data refers to the simulation of the beamline, whereas reconstructed data refers to the simulation of the detector reconstruction of this data. Simulating reconstructions is performed by GEANT4, a modelling program, which models how the interactions might appear in the detectors. In this simulation ‘parameterised reconstruction’ is used to estimate detector limitations, as the detector is not operational yet. Therefore, comparisons can be made in the simulation to judge how effectively the NDLaR and NDGAr can reconstruct data. The beamline magnetic horn can be switched between FHC (neutrino rich) and RHC (antineutrino rich)—the differences between these data sets when compared to the oscillated data at the FD will be crucial to determine the extent of CP violation in the leptonic sector.

With simulated events for the NDLaR and NDGAr in FHC and RHC arrangements stored as ROOT ntuples (a tree structured data format that contains many parameters and information for each simulated event) in CAFs (common analysis files). The data was taken from Fermilab servers and copied onto a server on the Edinburgh PPE network. This served was accessed via MacOs on a laptop, running XQuartz (for running graphical apps designed for Linux). Due to issues with accessing the server and directory names, it was necessary to run a container to run files using CAFÉ (CAF Environment—similar to ROOT but specific to analysing DUNE CAFs). The analysis framework, CAFAna, was used for the file analysis in this report as it is used for visualising the DUNE events. All editing was done using vim (an in command-line text editor), and the files were run in the container—no compiling was required as the CAFs were pre-processed and the software is designed to directly interpret the data (the analysis code is compiled once by the software, and the data processed at runtime).

Comparisons between the neutrino and antineutrino rich beams are made to examine the beam contents and comparisons between the detectors are made to analyse differences in how the same beam is recorded by the detectors. Comparisons between different types of interactions in the different detectors are made too. Finally the reconstructed data is compared to the truth data—differences are probed to discover how to mitigate such effects that can increase uncertainties.

3.1 Event Selection

CAFAna cuts were made to select appropriate channels. It was possible to also select an event by its final state. The $1\mu 1p$ final state was found by cutting all other particles: nuclear fragments, electromagnetic particles (γ , electrons), K^0 , $K^0 K^\pm$, π^0 , π^\pm and neutrons. $CC0\pi$ was found by only accepting charged current interactions with no pions in the final state.

⁴ROOT is an open-source software framework made at CERN used for data analysis mainly in particle physics [31]. It uses a C++ interpreter but also offers a python interface via PyROOT.

3.2 Reconstruction

Truth and reconstruction data was simulated by GENIE. Truth data was obtained in two forms—the simulated truth data and by energy conservation calculations. The formula used for true energy conservation is as follows:

$$E_{\nu}^{cons} = E_{\mu} + (E_p + m_p) - (m_n - E_b)$$

where E_b is the binding energy of nucleons in argon, E_p is the kinetic energy of the protons, E_{μ} is the energy of the muons, and $m_{p,n}$ are the proton and neutron masses.

Reconstructed data was also calculated the same way. In the analysis all reconstructed and true data used is from the CAFAna simulated values rather than these energy reconstruction formulae. There was however a third method for calculating reconstructions using the quasi-elastic reconstruction formula using reconstructed muon and proton energies:

$$E_{\nu}^{QE} = \frac{m_p^2 - (m_n - E_b)^2 - m_{\mu}^2 + 2(m_n - E_b)E_{\mu}}{2(m_n - E_b - E_{\mu} + p_{\mu} \cos \theta_{\mu})}$$

$p_{\mu} \cos \theta_{\mu}$ represents the muon momentum parallel to the beam, and m_{μ} is the muon mass.

3.3 Code

For a more technical explanation of the code please visit <https://github.com/paolominhas/CPV-DUNE-ND> [33].

4 Analysis and Discussion

4.1 Neutrino Energy Spectra

As DUNE searches for both muon neutrino disappearance and electron neutrino appearance, spectra of these channels (and antineutrino) are produced. Figure 12 shows the beam in FHC as detected at the NDGAr. Muon neutrinos make up the majority of the beam, as is expected in FHC. This sample contained 10^{17} events, and the histogram has 40 bins. There is a peak of muon neutrinos at relatively low energy (around 2 GeV). The most abundant background is made up of anti-muon neutrinos. This is likely due to wrong sign pions (this also applies to kaons) in the initial beams. Both positive and negative pions are produced in the beam, and decay to neutrinos and anti-neutrinos respectively. The magnetic horn will divert the negative pions away in FHC however not all can be diverted and as the pions are abundant at first a small proportion remains, decaying to anti-muon neutrinos. There are at least an order of magnitude less anti-muon neutrinos than muon neutrinos however and this is most noticeable by looking at the logarithmic y-axis.

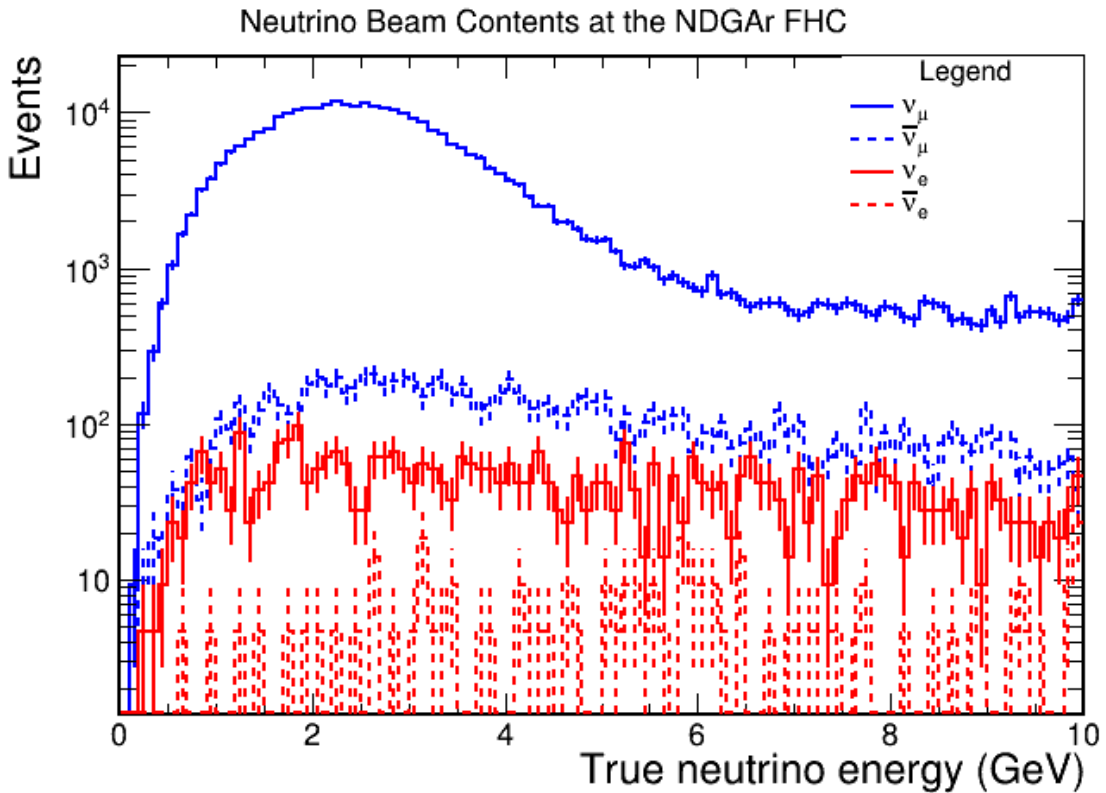


Figure 12: Simulating the true neutrino energy of the beam in FHC arrangement as seen by the NDGAr. Error bars have been added to show the error size relative to the energy values. It can be seen that errors in anti-electron neutrinos make are very large, as the proportion of them present is low. The logarithmic y-axis scale means the error bars on muon neutrinos are almost imperceptible on this figure.

The combinations of detector and magnetic horn arrangement were then compared.

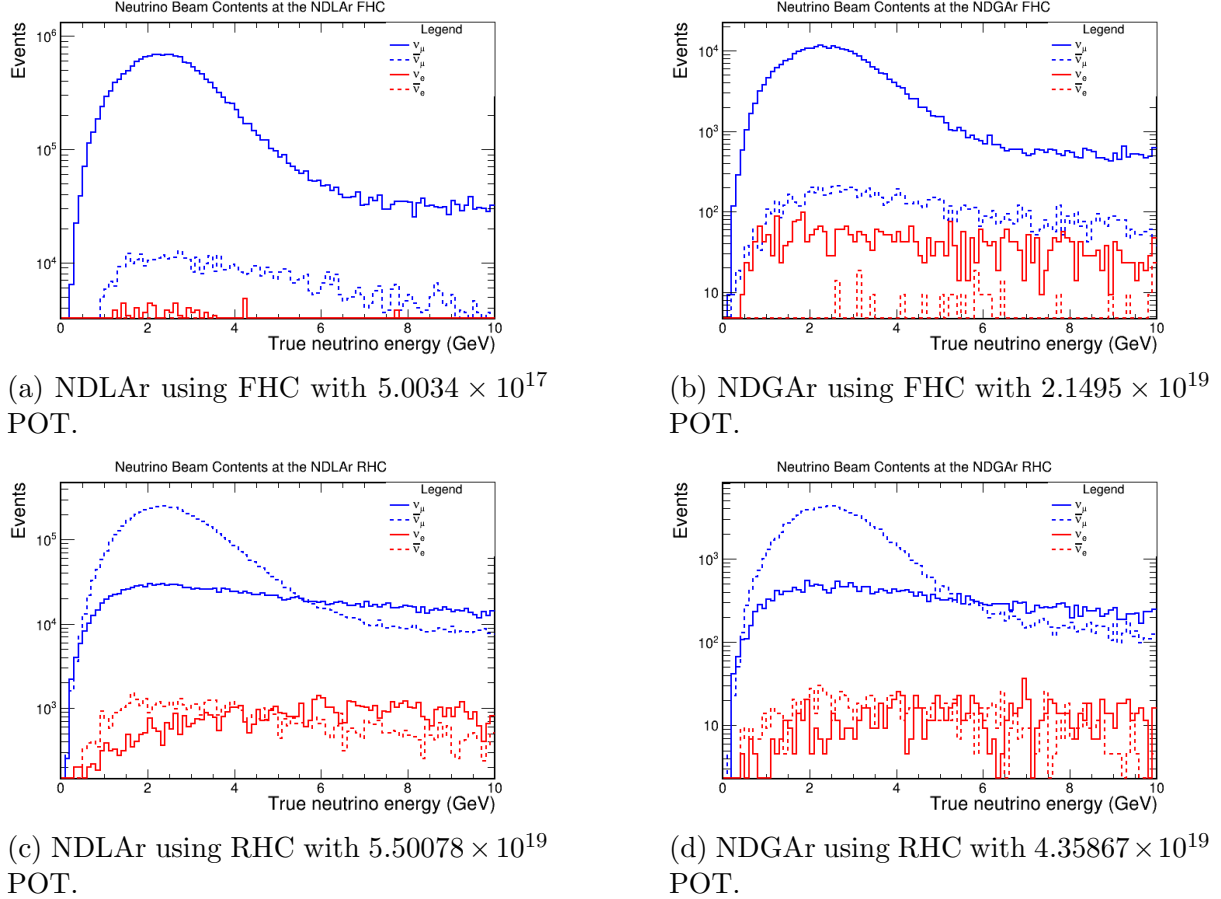


Figure 13: Comparison of ν_μ , ν_e , $\bar{\nu}_e$ and $\bar{\nu}_\mu$ energy spectra with different magnetic horn arrangement (FHC or RHC) and on the NDLAr and NDGAr detectors. The RHC arrangements (c & d) show a higher proportion of muon neutrinos than anti-muon neutrinos at higher energies. POT refers to the number of protons on target, a way of expressing how many relative events have occurred—a 5 month run at MINERVA, a past neutrino experiment, had around 10^{20} POT.

The RHC beams have higher backgrounds (unwanted neutrino channels) than the FHC beams. This is most evident at high neutrino energies, where there are more muon neutrinos than muon anti-neutrinos. This overlap is due to the amounts of π^+ and π^- particles produced by LBNF—there are more π^+ produced (see Table 1. The RHC diverts the π^+ particles away from the beam; however, at higher energies, where the pions have much larger momenta, it becomes difficult to divert these particles. Furthermore, at higher energies the pions tend to travel straighter (more parallel to the beam direction), meaning there is less of a horizontal component to amplify to deflect the π^+ . As there are more π^+ in the beam than π^- to start with, even though many are deflected, at high energies this is not enough. There is therefore a discrepancy between the symmetries of the neutrino and anti-neutrino beam; however, this is not caused by CP violation, but the nature of beam production. This can make comparing the two beams more complex, and emphasises how important it is to correctly detect these beams at the ND before the neutrinos oscillate.

4.2 Types of Interaction

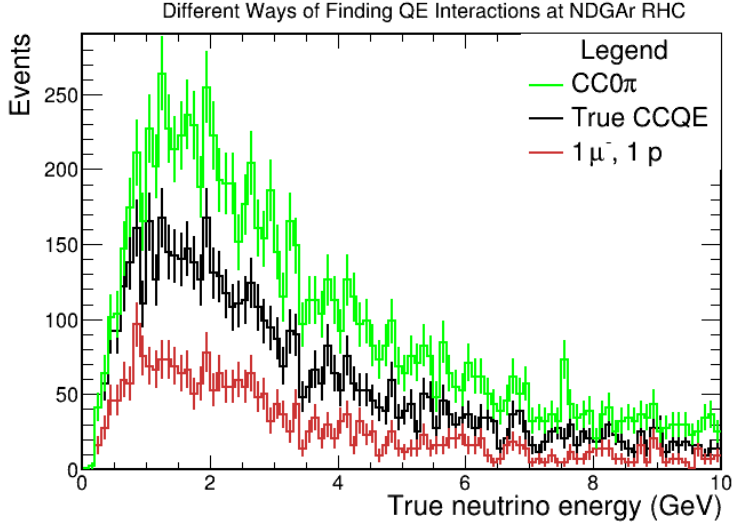


Figure 14: The types of interaction present in the NDGAr RHC. Error bars are larger than before as a low number of events is detected as we are recording ν_μ events in a $\bar{\nu}_\mu$ rich mode.

The true energy spectrum was divided in terms of the different interactions using a stacked histogram. This shows the proportions of each interaction type as a part of all interactions.

Three different approaches for calculating the neutrino energy in CCQE collisions in Figure 14. CC0 π shows the most events, and 1 μ^- 1 π has the lowest proportion of events. This is due to the fact that CCQE events are not the only source of a CC0 π final state and that 1 μ^- 1 π is not the only final state of CCQE interactions.

It was crucial to include all available data due to the prevalence of random errors in the data due to the random nature of decays and probability of detection (compounded by the various aforementioned systematic uncertainties).

This becomes more apparent by splitting the CC0 π final state into a larger range of interactions.

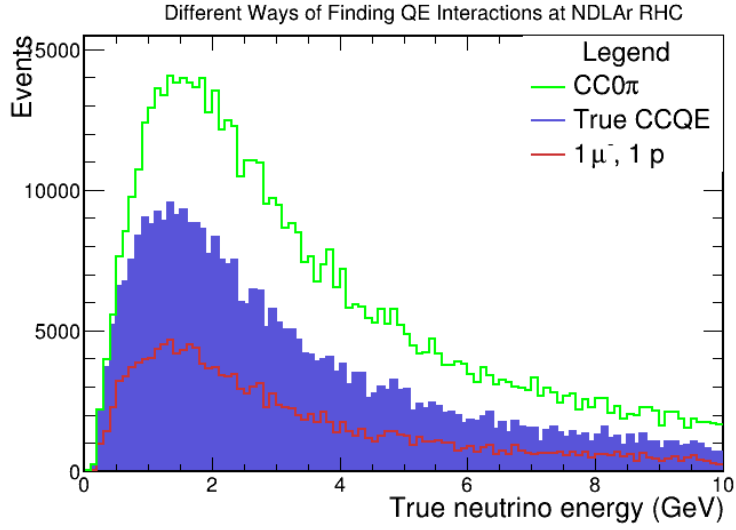


Figure 15: The same detector setup as Figure 14 however with a factor of 10 less data files – noticeably random errors have a greater impact on the spectrum. To reduce uncertainties very long periods of data taking are required to take more data.

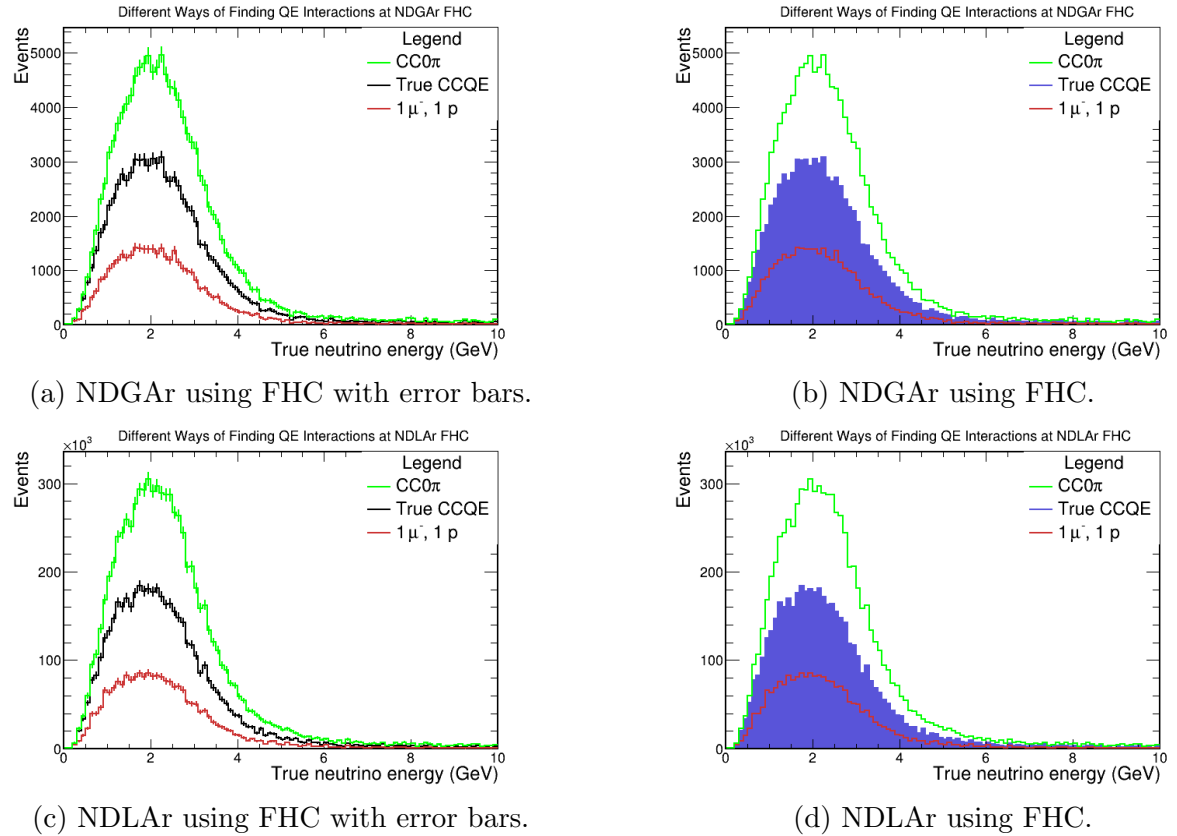
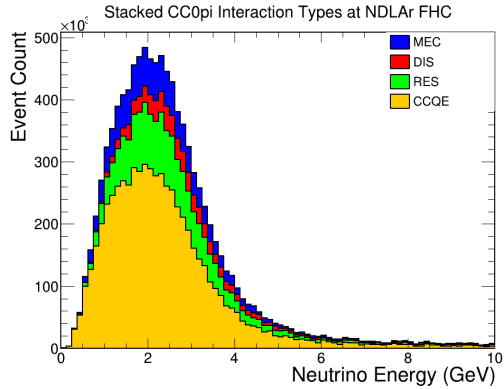
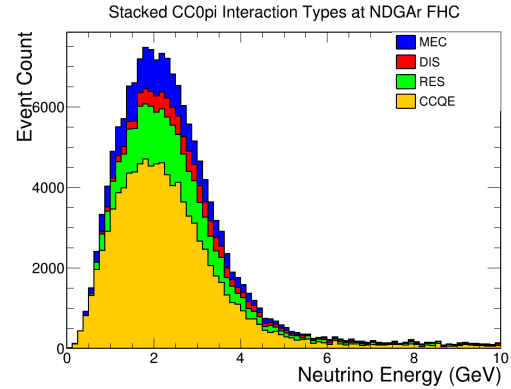


Figure 16: A comparison of the NDLaR and NDGAr in FHC. Both spectra show the same result.



(a) NDLAr using FHC.



(b) NDGAr using FHC.

Figure 17: The types of interaction present in the $\text{CC}0\pi$ final state, split into DIS, RES, MEC and CCQE interactions.

4.3 Approaches to Reconstruction

The reconstructions were calculated using various methods. The effectiveness of these methods to reconstruct CCQE events was at first analysed by comparing the energy spectra for these methods, against the true energy.

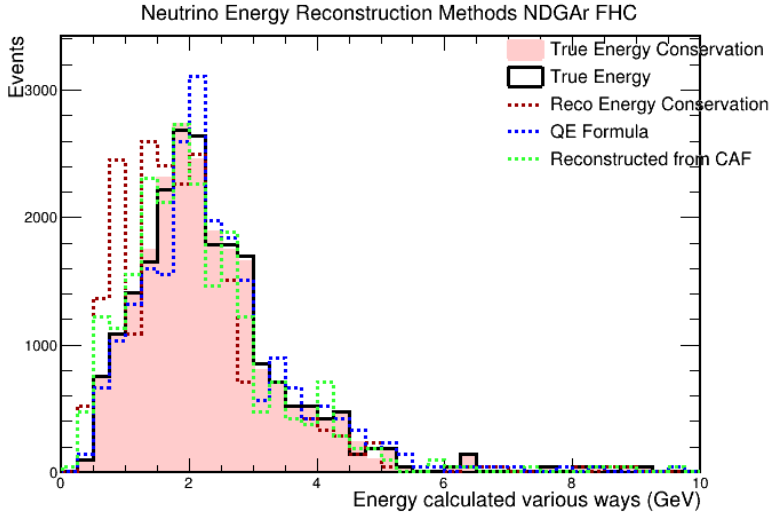


Figure 18: Different methods of calculating the reconstructions and energy for the NDGAr with FHC. True energy conservation and reco energy conservation are constructed using 4 momentum conservation in a CCQE interaction with a nucleus, for true and reconstruction energies respectively. The true energy (black) and reconstruction (green) are calculated but the CAF simulation. The QE formula uses the rest energies of the muon and proton formed in the collision to calculate the reconstructed energy.

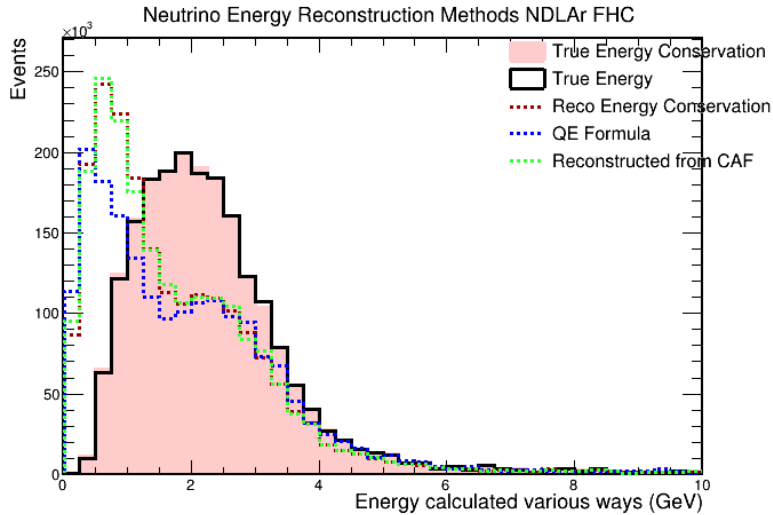


Figure 19: NDLAr in FHC has a particularly inaccurate reconstruction. The peak is at far lower energy and is higher. This means particles with lower energy in greater abundance are being detected. This can happen with tracks for a single particle being misidentified as two track (therefore two particles) if there is a gap in the middle of the track. This leads to more particles with lower energies being reconstructed. It appears this is more prevalent in the NDLAr than the NDGAr. This is due to the there being more FSI in the NDLAr due to the higher density of the medium, and the nuclei being more tightly bound.

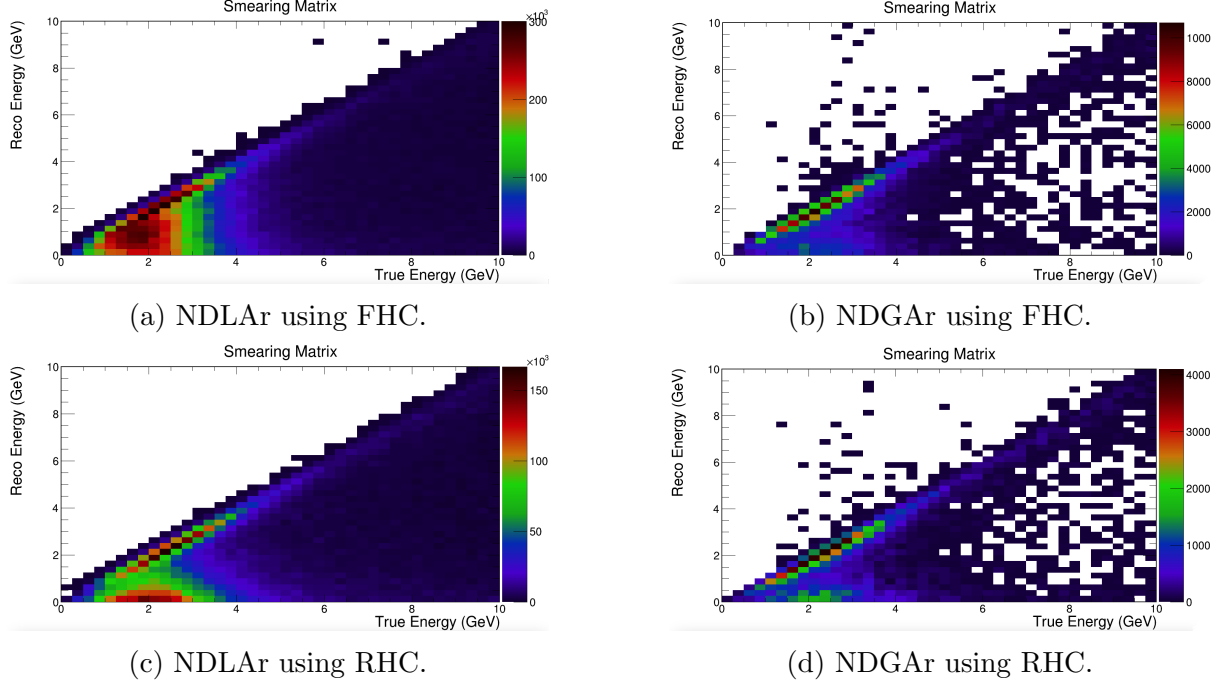


Figure 20: Comparison of ν_μ , ν_e , $\bar{\nu}_e$ and $\bar{\nu}_e$ true energy to reconstructed energy spectra with different magnetic horn arrangement (FHC or RHC) and on the NDLAr and NDGAr detectors. The NDLAr shows large differences in concentrations of reconstructions incorrectly

4.4 Truth versus Reconstructed Energy

The NDGAr RHC smearing matrix of truth and reconstructed energies (in Figure 20) using energy conservation formulas shows a clear linear relationship, which suggests similar energy values for the truth and reconstructed spectra. The reconstruction seems to mostly underestimate the energies rather than overestimate the energies – it mostly misidentifies higher energy truth events with a lower energy – hence explaining why at higher energies the concentration of events along the $y=x$ line is lower, as more high energy events have been identified as more low energy events.

By focussing on particular processes it can be possible to determine where these errors originate from. Therefore, it is also possible that 2p2h final states are becoming confused with CCQE—to investigate this the MEC spectrum (as well as the other interaction types) was further explored.

Neutron kinetic energy is difficult to detect—and as neutrons are effectively invisible in these detectors (do not leave visible ionisation tracks). This energy is not deposited in the detector and therefore is missing.

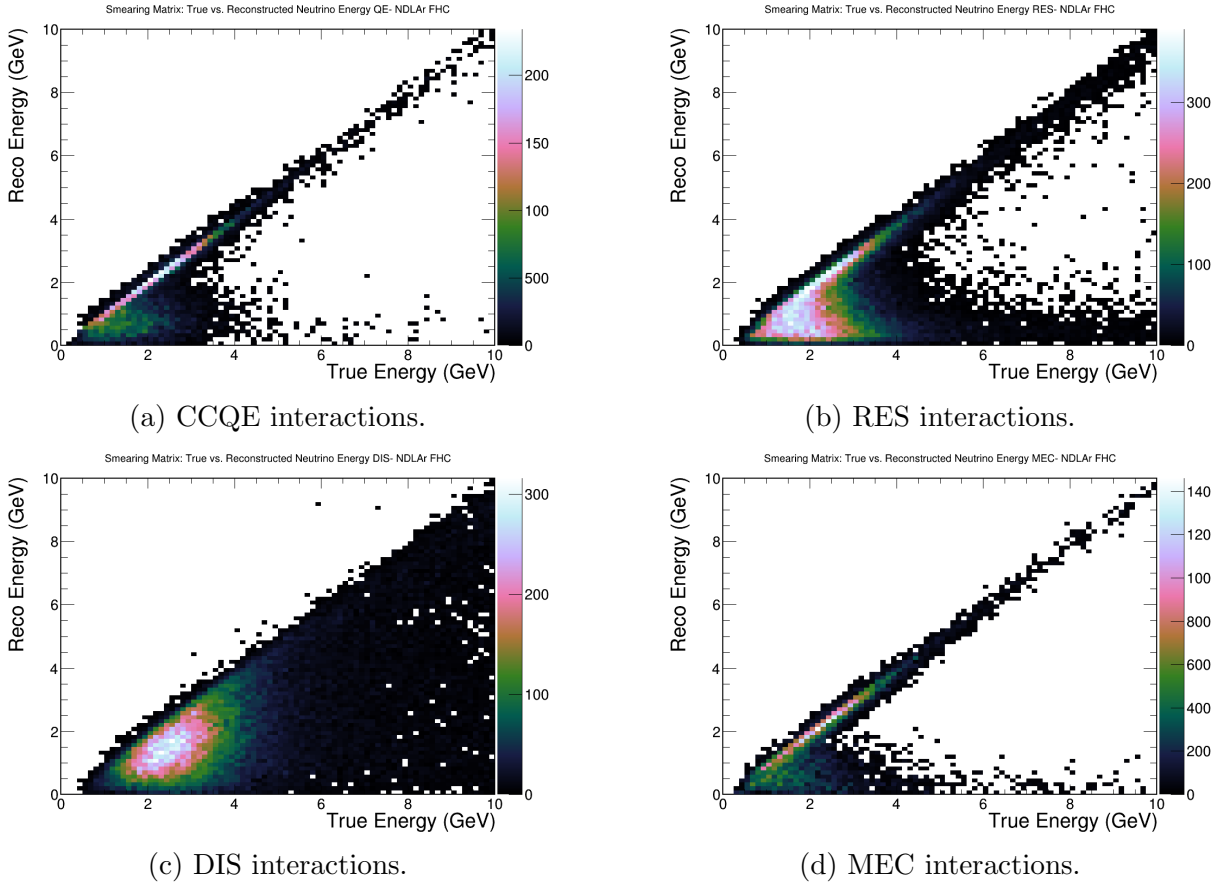


Figure 21: True versus reconstructed energy smear matrices for CCQE, RES, DIS and MEC interactions at NDLAr in FHC mode.

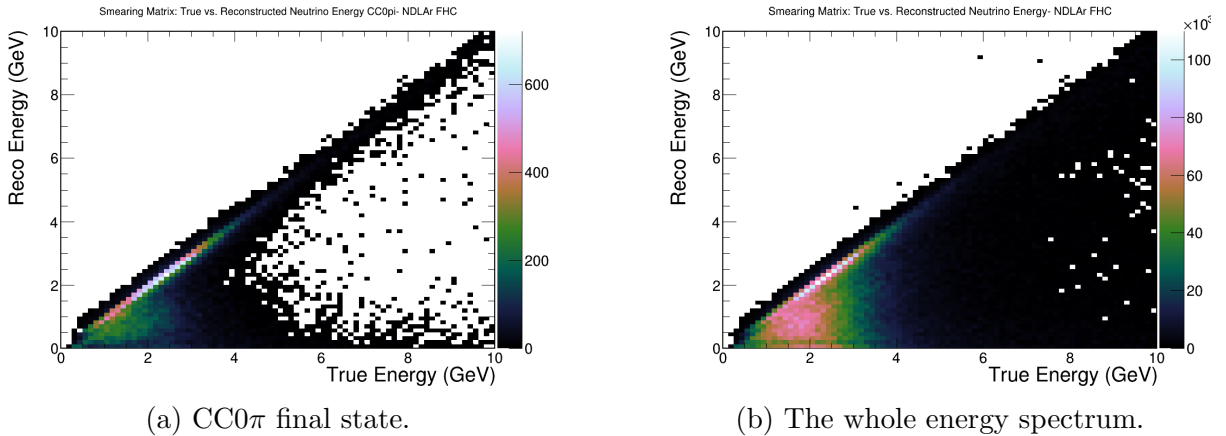


Figure 22: True versus reconstructed energy smear matrices for CC 0π final state and for all interactions at NDLAr in FHC mode. It is clear that reconstruction by selecting only CC 0π is better than that for taking the spectrum and attempting to find CCQE interactions, as can be seen by the greater saturation on the $y=x$ line on the CC 0π graph, with the absence of the erroneous concentration at 2 GeV. This is due to 2p2h and FSi being taken into account, in that by looking at the final state these are included.

5 Conclusions

DUNE ND simulations show difficulties in accurately reconstructing some neutrino interactions. In a bid to avoid using Monte Carlo simulations, like those in this report, to make up for this, it is possible to focus on particular interactions with better reconstructions to search for CP violation.

This report has shown that the NDGAr is necessary to be used in conjunction with the NDLAr—the shortcomings of the NDLAr were most visible in the energy reconstructions with large peaks at low energy. These were found to be due to neutrons escaping the detector. In order to accurately reconstruct ND spectra to predict FD spectra, the low energy region of the GAr is to be utilised.

The use of signatures rather than interactions to show results provides more useful results. The CC0 π final state is inclusive of 2p2h final states, as well as accounting for FSI. This leads to better reconstructions.

DUNE will improve the ND in the next decade to further constrain CPV, and depending on the value of δ_{CP} , obtain the value to a high degree of accuracy (see Figure ??). DUNE will have to move forward utilising different analysis techniques, as due to funding constraints the NDGAr has been removed from the baseline. One of the improvements made in the future may be to include a GArTPC, however this is uncertain. This outlines the challenge of funding in particle physics—large projects like DUNE require large sums of money. This report has shown that being aware of uncertainties and using simulations, it is possible to attempt to make up for less sophisticated detector technology. In this sense there is no doubt DUNE will make fascinating discoveries for decades to come.

References

- [1] W. Buchmüller, R.D. Peccei, and T. Yanagida. Leptogenesis as the origin of matter. *Annual Review of Nuclear and Particle Science*, 55(1):311–355, December 2005.
- [2] CERN. First particle tracks seen in prototype for international neutrino experiment, 2018.
- [3] J. H. Christenson, J. W. Cronin, V. L. Fitch, and R. Turlay. Evidence for the 2π decay of the k_2^0 meson. *Phys. Rev. Lett.*, 13:138–140, Jul 1964.
- [4] A. D. Sakharov. Violation of CP Invariance, C asymmetry, and baryon asymmetry of the universe. *Pisma Zh. Eksp. Teor. Fiz.*, 5:32–35, 1967.
- [5] Vyacheslav Galymov. An Overview of the Searches for the Violation of the Charge-Parity Symmetry in the Leptonic Sector. *Symmetry*, 16(1):130, 2024.
- [6] W. Pauli. Dear radioactive ladies and gentlemen. *Phys. Today*, 31N9:27, 1978.
- [7] Enrico Fermi. Tentativo di una teoria dei raggi β . *Il Nuovo Cimento (1924-1942)*, 11(1):1–19, 1934.
- [8] Fred Wilson. Fermi’s theory of beta decay. *American Journal of Physics*, 36:1150, 1968.
- [9] K.M. Case. Reformulation of the majorana theory of the neutrino. *Physical Review*, 107(1):307 – 316, 1957. Cited by: 114.
- [10] Samoil Bilenky. Neutrinos: Majorana or dirac? *Universe*, 6:134, 2020.
- [11] Benjamin J. P. Jones. The Physics of Neutrinoless Double Beta Decay: A Beginners Guide. *PoS*, TASI2020:007, 2021.
- [12] B. Pontecorvo. Neutrino Experiments and the Problem of Conservation of Leptonic Charge. *Zh. Eksp. Teor. Fiz.*, 53:1717–1725, 1967.
- [13] Ivan Esteban, M. C. Gonzalez-Garcia, Michele Maltoni, Thomas Schwetz, and Albert Zhou. The fate of hints: updated global analysis of three-flavor neutrino oscillations. *Journal of High Energy Physics*, 2020(9):178, 2020.
- [14] Ivan Esteban, M. Gonzalez-Garcia, Michele Maltoni, Ivan Martinez-Soler, João Pinenheiro, and Thomas Schwetz-Mangold. Nufit-6.0: Updated global analysis of three-flavor neutrino oscillations. 2024.
- [15] C. Marshall. P5 townhall meeting, dune far detectors—phase ii, 2023.
- [16] Vaia Papadimitriou. Design of the LBNF Beamline. In *38th International Conference on High Energy Physics*, 2017.
- [17] B. Abi et. al. Volume i. introduction to dune. *Journal of Instrumentation*, 15(08):T08008, 2020.

- [18] A. Aduszkiewicz et. al. Measurements of hadron production in $\pi^+ + \text{C}$ and $\pi^+ + \text{Be}$ interactions at 60 GeV/c. *Phys. Rev. D*, 100:112004, 2019.
- [19] B. Abi et. al. Deep underground neutrino experiment (dune), far detector technical design report, volume ii: Dune physics, 2020.
- [20] Pantelis Melas, Dimitrios K. Papoulias, and Niki Saoulidou. New physics opportunities at the dune near detector. *Particles*, 7(3):623–633, 2024.
- [21] Igor Krasnov. Dune prospects in the search for sterile neutrinos. *Phys. Rev. D*, 100:075023, 2019.
- [22] Valentina De Romeri, Kevin J. Kelly, and Pedro A. N. Machado. Dune-prism sensitivity to light dark matter. *Phys. Rev. D*, 100:095010, 2019.
- [23] C. Patrick. Introduction to neutrino interactions, 2021.
- [24] Daniel Z. Freedman. Coherent effects of a weak neutral current. *Phys. Rev. D*, 9:1389–1392, 1974.
- [25] Jiajun Liao and Danny Marfatia. Coherent constraints on nonstandard neutrino interactions. *Physics Letters B*, 775:54–57, 2017.
- [26] M. Abdullah et. al. Coherent elastic neutrino-nucleus scattering: Terrestrial and astrophysical applications, 2022.
- [27] R Pradhan, R Lalnuntluanga, and A Giri. Probing neutrino-nucleus interaction in dune and microboone. 2024.
- [28] E. A. Paschos and Dario Schalla. Pion production by neutrinos in the delta resonance region and possible application to CP searches. 2012.
- [29] Keping Xie, Jun Gao, T.J. Hobbs, Daniel R. Stump, and C.-P. Yuan. High-energy neutrino deep inelastic scattering cross sections. *Physical Review D*, 109(11), June 2024.
- [30] J.W Van Orden and T.W Donnelly. Mesonic processes in deep-inelastic electron scattering from nuclei. *Annals of Physics*, 131(2):451–493, 1981.
- [31] R. Brun and F. Rademakers. ROOT: An object oriented data analysis framework. *Nucl. Instrum. Meth. A*, 389:81–86, 1997.
- [32] Costas Andreopoulos, Christopher Barry, Steve Dytman, Hugh Gallagher, Tomasz Golan, Robert Hatcher, Gabriel Perdue, and Julia Yarba. The genie neutrino monte carlo generator: Physics and user manual, 2015.
- [33] P. Minhas. Cpv-dune-nd repository, 2025.

A The PNMS Matrix and Oscillation Probabilities

The PNMS matrix itself can be expressed by three rotation matrices as well as three complex phases:

$$U_{\text{PMNS}} = \begin{bmatrix} 1 & 0 & 0 \\ 0 & c_{23} & s_{23} \\ 0 & -s_{23} & c_{23} \end{bmatrix} \begin{bmatrix} c_{13} & 0 & s_{13}e^{-i\delta_{CP}} \\ 0 & 1 & 0 \\ -s_{13}e^{i\delta} & 0 & c_{13} \end{bmatrix} \begin{bmatrix} c_{12} & s_{12} & 0 \\ -s_{12} & c_{12} & 0 \\ 0 & 0 & 1 \end{bmatrix} \begin{bmatrix} 1 & 0 & 0 \\ 0 & e^{i\beta} & 0 \\ 0 & 0 & e^{i\gamma} \end{bmatrix} \quad (12)$$

where $c_{ij} = \cos \theta_{ij}$ and $s_{ij} = \sin \theta_{ij}$, δ_{CP} refers to the CP violation phase and β, γ are the Majorana phases.

The first three matrices represent the 12-sector, 13-sector and 23-sector respectively, the indices referring to the relationships between mass eigenstates of those indicies. It is clear that the CP-violation terms are introduced in the 13-sector. These matrices are then multiplied to find the matrix elements:

$$U_{\text{PMNS}} = \begin{bmatrix} c_{12}c_{13} & s_{12}c_{13} & s_{13}e^{-i\delta} \\ -s_{12}c_{23} - c_{12}s_{23}s_{13}e^{i\delta} & c_{12}c_{23} - s_{12}s_{23}s_{13}e^{i\delta} & s_{23}c_{13} \\ s_{12}s_{23} - c_{12}c_{23}s_{13}e^{i\delta} & -c_{12}s_{23} - s_{12}c_{23}s_{13}e^{i\delta} & c_{23}c_{13} \end{bmatrix} \begin{bmatrix} 1 & 0 & 0 \\ 0 & e^{i\beta} & 0 \\ 0 & 0 & e^{i\gamma} \end{bmatrix} \quad (13)$$

The first of these complex phases is δ_{CP} . The terms $e^{i\beta}$ and $e^{i\gamma}$ refer to the 'Majorana phases'—these additional phases will be present if neutrinos are Majorana particles, however do not impact neutrino oscillation and henceforth can be ignored in this paper. Therefore the PNMS matrix is simplified to:

$$U_{\text{PMNS}} = \begin{bmatrix} c_{12}c_{13} & s_{12}c_{13} & s_{13}e^{-i\delta} \\ -s_{12}c_{23} - c_{12}s_{23}s_{13}e^{i\delta} & c_{12}c_{23} - s_{12}s_{23}s_{13}e^{i\delta} & s_{23}c_{13} \\ s_{12}s_{23} - c_{12}c_{23}s_{13}e^{i\delta} & -c_{12}s_{23} - s_{12}c_{23}s_{13}e^{i\delta} & c_{23}c_{13} \end{bmatrix} \quad (14)$$

By finding the probability of transferring between states (by squaring the second state acting upon the first) it is possible to derive the appearance and disappearance probabilities that are of interest at DUNE:

$$\begin{aligned} P(\nu_\mu \rightarrow \nu_e) \approx & \sin^2 \theta_{23} \sin^2 2\theta_{13} \frac{\sin^2 \Delta_{31}(1-A)}{(1-A)^2} \\ & + \alpha \cos \theta_{13} \sin 2\theta_{12} \sin 2\theta_{13} \sin 2\theta_{23} \frac{\sin \Delta_{31}(1-A) \sin \Delta_{31}A}{(1-A)A} \\ & + \alpha^2 \cos^2 \theta_{23} \sin^2 2\theta_{12} \frac{\sin^2 \Delta_{31}A}{A^2} \\ & \pm \delta_{CP} \sin \delta \cos \theta_{13} \sin 2\theta_{12} \sin 2\theta_{13} \sin 2\theta_{23} \frac{\sin \Delta_{31}(1-A) \sin \Delta_{31}A}{(1-A)A} \end{aligned} \quad (15)$$

$$P(\nu_\mu \rightarrow \nu_\mu) \approx 1 - \sin^2 2\theta_{23} \sin^2 \Delta_{31} + 4\alpha \cos^2 \theta_{13} \sin^2 \theta_{23} \sin 2\theta_{12} \cos \Delta_{31} \sin \Delta_{31} \frac{\sin \Delta_{31} A}{A} \quad (16)$$

where:

$$\Delta_{31} = \frac{\Delta m_{31}^2 L}{4E}$$

$$A = \frac{2\sqrt{2}G_F N_e E}{\Delta m_{31}^2}$$

$$\alpha = \frac{\Delta m_{21}^2}{\Delta m_{31}^2}$$

- $\theta_{12}, \theta_{13}, \theta_{23}$ are neutrino mixing angles
- δ_{CP} is CP-violating phase
- $\Delta m_{31}^2, \Delta m_{21}^2$ are mass-squared differences
- L : baseline length (1300 km for DUNE).
- E : neutrino energy
- G_F : Fermi constant
- N_e : electron number density in matter

The first equation describes the appearance probability $P(\nu_\mu \rightarrow \nu_e)$, which is sensitive to CP violation and matter effects (via A). The second equation describes the disappearance probability $P(\nu_\mu \rightarrow \nu_\mu)$, which determines the atmospheric mixing angle θ_{23} .